The Cryosphere
Discussions

Evaluating Simplifications of Subsurface Process Representations for Field-scale Permafrost Hydrology Models

Bo Gao, Ethan T. Coon

Environmental Sciences Division, Oak Ridge National Laboratory, Oak Ridge, Tennessee, USA

Correspondence to: Ethan T. Coon (coonet@ornl.gov)

Abstract. Permafrost degradation within a warming climate poses a significant environmental threat through both the permafrost carbon feedback and damage to human communities and infrastructure. Understanding this threat relies on better understanding and numerical representation of thermo-hydrological permafrost processes, and the subsequent accurate prediction of permafrost dynamics. All models include simplified assumptions, implying a tradeoff between model complexity and prediction accuracy. The main purpose of this work is to investigate this tradeoff when applying the following commonly made assumptions: (1) assuming equal density of ice and liquid water in frozen soil; (2) neglecting the effect of cryosuction in unsaturated freezing soil; and (3) neglecting advective heat transport during soil freezing and thaw. This study designed a set of 62 numerical experiments using the Advanced Terrestrial Simulator (ATS v1.2) to evaluate the effects of these choices on permafrost hydrological outputs, including both integrated and pointwise quantities. Simulations were conducted under different climate conditions and soil properties from three different sites in both column- and hillslope-scale configurations. Results showed that amongst the three physical assumptions, soil cryosuction is the most crucial yet commonly ignored process. Neglecting cryosuction, on average, can cause 10% ~ 20% error in predicting evaporation, 50% ~ 60% error in discharge, 10% ~ 30% error in thaw depth, and 10% ~ 30% error in soil temperature at 1 m beneath surface. The prediction error for subsurface temperature and water saturation is more obvious at hillslope scales due to the presence of lateral flux. By comparison, using equal ice-liquid density has a minor impact on most hydrological variables, but significantly affects soil water saturation with an averaged 5% ~ 15% error. Neglecting advective heat transport presents the least error, 5% or even much lower, in most variables for a general Arctic tundra system, and can decrease the simulation time at hillslope scales by 40% ~ 80%. By challenging these commonly made assumptions, this work provides permafrost hydrology modelers important context for better choosing the appropriate process

The Cryosphere
Discussions

30   representation for a given modeling experiment.

31

32   **Copyright Statement.** This manuscript has been authored by UT- Battelle, LLC under Contract

33   No. DE-AC05-00OR22725 with the U.S. Department of Energy. The United States Government

34   retains and the publisher, by accepting the article for publication, acknowledges that the United

35   States Government retains a non-exclusive, paid-up, irrevocable, world-wide license to publish, or

36   reproduce the published form of this manuscript, or allow others to do so, for United States

37   Government purposes. The Department of Energy will provide public access to these results of

38   federally   sponsored   research   in   accordance   with   the   DOE   Public   Access   Plan

39   (http://energy.gov/downloads/doe-public-access-plan).

40   **1 Introduction**

41   Permafrost describes a state of ground which stays frozen continuously over multiple years, which

42   may cover an entire region (e.g., Arctic tundra) or occur in isolation (e.g., alpine top). From the

43   perspective of scope, permafrost occupies approximately 23.9% (22.79 million km^2) of the

44   exposed land area of the northern hemisphere (Zhang et al., 2008), as well as alpine regions and

45   Antarctica in the southern hemisphere. Permafrost areas store a vast amount of organic carbon, of

46   which most is stored in perennially frozen soils (Hugelius et al., 2014). If the organic carbon is

47   exposed due to permafrost thaw, it is likely to decay with microbial activity, releasing greenhouse

48   gas to the atmosphere and exacerbating global warming. In Arctic tundra, permafrost also plays

49   an important role in maintaining water, habitat of wildlife, landscape, and infrastructure (Berteaux

50   et al., 2017; Dearborn et al., 2021; Hjort et al., 2018; Sugimoto et al., 2002). Permafrost

51   degradation may cause significant damage to the local ecosystem, reshape the surface and

52   subsurface hydrology, and eventually influence the global biosphere (Cheng and Wu, 2007;

53   Jorgenson et al., 2001; Tesi et al., 2016; Walvoord and Kurylyk, 2016). Therefore, the occurrent

54   and potential impacts motivate the development of computational models with the goal of better

55   understanding the thermal and hydrological processes in permafrost regions, and to consequently

56   predict permafrost thaw more accurately.

57   Simulating soil freezing and thaw processes is a challenging task that incorporates mass and energy

58   transfer among atmosphere, snowpack, land surface (perhaps with free water), and a variably

59   saturated subsurface. Several hydrological models with different complexity and applicable scales

Should reference Grenier et al. 2018 (AWR) somewhere.

60   have been developed to investigate the complicated interactions. A comprehensive review of

61   permafrost models based on empirical and physical representations using analytical and numerical

62   solutions can be found in (Bui et al., 2020; Dall'Amico et al., 2011; Jan et al., 2020; Kurylyk et

63   al., 2014; Kurylyk and Watanabe, 2013; Riseborough et al., 2008). Process-rich models which aim

64   to predict permafrost change through direct simulation of mass and energy transport, such as

65   the Advanced Terrestrial Simulator (ATS; Painter et al., 2016), GEOtop (Endrizzi et al., 2014),

66   CryoGrid 3 (Westermann et al., 2016), PFLOTRAN-ICE (Karra et al., 2014), and SUTRA-ICE

67   (McKenzie et al., 2007), have been demonstrated to describe thermal permafrost hydrology under

68   various climate conditions. Nominally, representing more physical process complexity should

69   improve accuracy, but how much accuracy and at what computational expense (and therefore

70   tradeoff in ability to run larger, or larger ensembles of, simulations) is not always theoretically

71   known. Thus, certain assumptions or simplifications about the system are a significant part of

72   model development.

73   Even in the most process-rich models of permafrost change, three such physics simplifications are

74   often made: representing water at constant density (thereby neglecting the expansion of ice relative

75   to liquid water), neglecting cryosuction of water in unsaturated, partially frozen soils, and

76   neglecting advective heat transport.

77   First, because of the lower density of ice than liquid water, freezing water must expand the volume

78   of the porous media, push liquid water into nearby volume, or otherwise expand the volume

79   occupied by that water. As all of the current set of models operate under the assumption of a rigid

80   solid matrix and thus the absence of mechanical equations describing matrix deformation or frost

81   heave, including this expansion typically results in large pressures that must be offset by grain

82   compressibility or another mechanism. Therefore, the densities of ice and liquid water are

83   frequently assumed equal (e.g., Dall'Amico et al., 2011; Devoie and Craig, 2020; Weismüller et

84   al., 2011). It is uncertain whether this simplification affects predictions of permafrost change and

85   thermal hydrology.

86   Second, cryosuction describes the redistribution of water in partially frozen, unsaturated soils

87   caused by increased matric suction. At the interface of ice and liquid water, negative pressures

88   result in the migration of liquid water toward the freezing front and the subsequent increase of ice

89   content. Several approaches representing cryosuction in models are used (Dall'Amico et al., 2011;

90   Noh et al., 2012; Painter and Karra, 2014; Stuurop et al., 2021), either in an empirical form or

Not all models... ex Comsol

91   physically derived from the generalized Clapeyron equation. Other process-rich models have

92   ignored cryosuction entirely (McKenzie et al., 2007; Viterbo et al., 1999). Dall'Amico et al.

93   (2011), Painter (2011) and Painter and Karra (2014) evaluated their respective Clapeyron equation

94   based cryosuction models in soil column freezing simulations and presented a good match between

95   simulations and laboratory experiments in total water content (liquid and ice). Recently, Stuurop

96   et al. (2021) applied an empirical expression, a physics-based expression, and no cryosuction in

97   simulating soil column freezing process. They compared the simulated results with observations

98   from laboratory experiments. This comparison demonstrated minor differences between empirical

99   and Clapeyron-based cryosuction expressions, but the simulation without cryosuction cannot

100 predict the distribution of total water content in a laboratory-scale soil column. To our knowledge,

101 there is still no literature showing the effect of cryosuction on plot-scale permafrost predictions.

102 Third, heat transport in process-rich models is described using an energy conservation equation,

103 mainly including heat conduction, latent heat exchange, and heat advection. From a continuum-

104 scale perspective, conductive heat transport is expressed in the form of a diffusive term based

105 on Fourier's law. Latent heat exchange accompanies phase change which alters the system enthalpy.

106 Advective heat transport describes the energy exchange caused by the flow of liquid water driven

107 by a hydraulic gradient (i.e., forced convection), which is expressed through an advective term in

108 energy balance equations. Additionally, other mechanisms that control heat transport, such as

109 water vapor movement, thermal dispersion, radiant energy, etc., are neglected by nearly all models

110 of permafrost and are not considered here. Among these heat transport mechanisms, it is

111 commonly recognized [assumed] that heat conduction predominates heat transport in the subsurface (Nixon,

112 1975). However, there are also studies demonstrating the importance of advective heat transport

113 in permafrost hydrology through field observation analysis or modeling comparison. Such

114 situations where advective heat makes [transport] important contributions roughly fall into three categories.

115 The first centers on the development of taliks beneath lakes, ponds, snowmelt water and rainfall

116 induced runoff, or in the existence of supra-/sub-permafrost groundwater flow (e.g., Luethi et al.,

117 2017; McKenzie and Voss, 2013; Rowland et al., 2011). The second focuses on microtopographic

118 features that focus significant amount of water flux through small areas. This includes both low-

119 center ice wedge polygons associated with the formation of thermokarst ponds (e.g., Abolt et al.,

120 2020; Harp et al., 2021) and thermo-erosion gullies (e.g., Fortier et al., 2007; Godin et al., 2014).

121 In these cases, large, focused flows across small spatial scales allow advective heat transport to

[Handwritten margin notes:]
X 111, 112 — assumed; too old to use for saying "commonly assumed" which implies more recent cases.
114 — transport
118 — (significant amount of water flux)
Bracket lines 114–121: See also Dagenais et al 2020 (Hydrogeology J.), Liu et al 2022 (WRR), (Talik 3D model) (comparison of Conduction vs Advection-Conduction at a real site)

122 dominate. The last category includes those studying the construction and maintenance of

123 infrastructure influenced by groundwater flow (e.g., Chen et al., 2020). Thus, these studies focus

124 on either location-specific or scale-limited problems. As McKenzie and Voss (2013) stated,

125 whether heat advection outweighs heat conduction depends on soil permeability, topography, and

126 groundwater availability. Relative to these special cases, we are more interested in to what extent

127 advective heat transport associated with liquid water flow contributes to permafrost hydrologic

128 change in a hillslope-scale or larger Arctic system.

129 To clarify the significant differences in model representations of permafrost, we investigate the

130 influence of including or not including these processes on permafrost change at plot-to-hillslope

131 scales. We take the advantage of the flexibility offered by ATS to express multiple options of

132 process representation to implement this study in numerical experiments. For ice density, we

133 compare simulations with and without differences in ice density relative to water density; for

134 cryosuction, we compare simulations using a Clapyron equation-based expression and excluding

135 the cryosuction effect; and for heat transport, we compare simulations including or neglecting

136 advective heat transport. All comparisons are carried out across a range of Arctic climate

137 conditions and soil properties from three different sites. Both 1D soil-column-scale and 2D

138 hillslope-scale models are considered, in which varying hillslope geometries (i.e.,

139 convergent/divergent hillslope) and aspects (i.e., north/south) are included. The aim of this study

140 is to provide permafrost hydrology modelers with crucial comparisons for better choosing a model

141 representation for a given study by formally considering the tradeoff between model complexity,

142 accuracy, and, at least for one code, performance.

143 **2 Theory**

144 The Advanced Terrestrial Simulator (ATS v1.2) (Coon et al., 2020) configured in permafrost mode

145 (Jan et al., 2018, 2020; Painter et al., 2016) was used to implement all numerical experiments in

146 this study. ATS is a process-rich code developed for simulating integrated surface and subsurface

147 hydrological processes, specifically capable of permafrost applications. It has been shown to

148 successfully compare to observations of seasonal soil freezing and thaw processes at different

149 scales. This includes 1D models of vertical energy transport typical of large-scale flatter regions

150 (Atchley et al., 2015), and 2D models admitting lateral flow and transport in Arctic fens (Sjöberg

151 et al., 2016), and polygonal ground (Jan et al., 2020).

152 The permafrost configuration of ATS comprises coupled water flow and energy transfer within
153 variably saturated soils and at land surfaces, a surface energy balance model describing thermal
154 processes in snow, and a snow distribution module for surface microtopography (Painter et al.,
155 2016). The subsurface system solves a three-phase (liquid, ice, gas), two-component (water vapor,
156 air) Richards-type mass balance equation with Darcy's law and an advection-diffusion energy
157 balance equation. The surface system includes an overland flow model with diffusion wave
158 approximation, and an energy balance equation with an introduced temperature-dependent factor
159 describing the effect of surface water freezing. The subsurface system and surface system are
160 coupled through the continuity of pressure, temperature, and the corresponding fluxes by
161 incorporating the surface equations as boundary conditions of the subsurface equations (Coon et
162 al., 2020). The evolution of a snowpack and its effect on the surface energy balance is described
163 using an energy balance approach based on a subgrid model concept that includes all major heat
164 fluxes at the land surface. For a more detailed description of the permafrost configuration and
165 implementation in ATS, as well as key mathematical equations, the reader is referred to Painter et
166 al. (2016). Changes in this "most complex" model of permafrost hydrology are enabled by the
167 Arcos multiphysics library leveraged in ATS; this allows the precise model physics to be specified
168 and configured at runtime through the use of a dependency graph describing swappable
169 components in the model physics (Coon et al., 2016).

170 **2.1 Ice density**

171 The density of ice (kg/m^3) is represented as a Taylor series expansion in both temperature and
172 pressure:

173 $$\rho_i = [a + (b + c\Delta T) \times \Delta T] \times (1 + \alpha\Delta p) \tag{1}$$

174 and the density of liquid water (kg/m^3) is represented as:

175 $$\rho_l = [a + (b + (c + d\Delta T) \times \Delta T) \times \Delta T] \times (1 + \alpha\Delta p) \tag{2}$$

176 where $\Delta T = T$ - 273.15, $\Delta p = p_l$ - 1e5, T and p_l are temperature (K) and liquid pressure (>101325
177 Pa), respectively; and a, b, c, d, α are constant coefficients, listed in Table 1. Under conditions of
178 equal density, we assume $\rho_i = \rho_l$.

179 **Table 1 Coefficients in density of ice and liquid**

	a	b	c	d	α
ρ_i	916.724	-0.147143	-2.38e-4	–	1.0e-10
ρ_l	999.915	0.0416516	-1.01e-2	2.06e-4	5.0e-10

180 **2.2 Cryosuction**

181 Painter and Karra (2014) proposed a constitutive relationship for phase partitioning of water in

182 frozen soils based on Clapeyron equation and Van Genuchten model (Van Genuchten, 1980):

183
$$
s_\text{l} = \begin{cases} S_*(-\beta\rho_\text{l}L_\text{f}\vartheta), \vartheta < \vartheta_\text{f} \\ S_*(p_\text{g}-p_\text{l}), \vartheta \geq \vartheta_\text{f} \end{cases}, \quad \vartheta = \frac{T(\text{K})-273.15}{273.15}, \quad \vartheta_\text{f} = -\frac{\psi_*(1-s_\text{g})}{\beta L_\text{f}\rho_\text{l}}
$$
$$
s_\text{i} = 1 - s_\text{l}/S_*(p_\text{g}-p_\text{l})
$$
(3)

184 where s_n is the saturation of n-phase and the subscripts $n =$ l, i, g are liquid, ice, and gas phases,

185 respectively; β is a coefficient; L_f is the heat fusion of ice; p_n ($n =$ l, g) is the pressure of n-phase;

186 S_* is the Van Genuchten model. This physically derived formulation can describe the change of

187 matric suction in the frozen zone due to the change of ice content, and thus has the capacity to

188 represent cryosuction.

189 Alternatively, to exclude the effect of cryosuction in this study, we used the Van Genuchten model

190 to determine the total water content, including liquid water and ice. The liquid water content is

191 achieved by an empirical relationship (soil-freezing characteristic curve) which describes that the

192 liquid water content only relates to temperature through an exponent function (McKenzie et al.,

193 2007).

194
$$
s_\text{l} = s_\text{r} + (s_\text{sat}-s_\text{r})\exp\left[-\left(\frac{T(\text{K})-273.15}{\omega}\right)^2\right]
$$
$$
s_\text{i} = S_*(p_\text{g}-p_\text{l})-s_\text{l}
$$
(4)

195 where s_r, s_sat are saturations of liquid water at residual and saturated conditions, respectively; ω is

196 a constant coefficient.

197 **2.3 Advective heat transport**

198 The energy conservation equation of the subsurface system is given by:

199
$$
\frac{\partial}{\partial t}\left[\phi\sum_{n=\text{l,i,g}}(\rho_n s_n u_n) + (1-\phi)c_\text{v,soil}T\right] + \underbrace{\nabla\cdot(\rho_\text{l}h_\text{l}\mathbf{V}_\text{l})}_{\text{advective heat}} \underbrace{-\nabla\cdot(\kappa_\text{e}\nabla T)}_{\text{conductive heat}} = Q_\text{E}
$$
(5)

200 where ϕ is porosity; u_n is the specific internal energy of phase ($n \in \{$l, i, g$\}$); $c_\text{v,soil}$ (J m^{-3} K^{-1}) is

201 the volumetric heat capacity of the soil grains. The second and third terms represent the advective

202 and conductive heat transport in subsurface, in which h_l (J/mol) is the specific enthalpy of liquid;

203 $\mathbf{V}_\text{l}$ (m/s) is the velocity vector of liquid water determined by Darcy's law; and κ_e (W m^{-1} K^{-1}) is

204 the effective thermal conductivity of the bulk material including soil, air, liquid water, and ice. Q_E

205 is the sum of all thermal energy sources (W/m^3).

206 Similarly, the energy balance equation of the surface system is:

207 $$\frac{\partial}{\partial t}\{[\chi\rho_l u_l + (1-\chi)\rho_i u_i]\delta_w\} + \underbrace{\nabla\cdot(h_l\chi\rho_l\delta_w\mathbf{U}_w)}_{\text{advective heat}} - \underbrace{\nabla\cdot\{[\chi\kappa_l + (1-\chi)\kappa_i]\delta_w\nabla T\}}_{\text{conductive heat}} = Q_{\text{net}} \qquad (6)$$

208 in which χ is the unfrozen fraction determined by surface temperature; δ_w is ponded depth (m);

[handwritten note: water]

209 $\mathbf{U}_w$ (m/s) is the velocity vector of liquid water on the surface determined by the diffusion-wave

210 approximated St. Venant equations (Gottardi and Venutelli, 1993) and Manning equation

211 (Wasantha Lal, 1998); κ_n (W m^{-1} K^{-1}) is the thermal conductivity of n-phase ($n = l, i$); Q_{net} (W/m^3)

212 is the net thermal energy into and out of surface, including that from solar radiation, rain and snow

[handwritten note: ground]

213 melt, water loss by evaporation and to the subsurface, and conductive and advected heat transport

214 to/from the subsurface. The second and third terms represent the (lateral) advective and conductive

215 heat transport that occur across the land surface.

216 3 Methods

217 To evaluate the impact of representation of ice density, cryosuction, and advective heat transport

218 in permafrost modeling under different climate conditions and soil properties, we selected three

219 sites for their variance in climactic condition: Utqiagvik (Barrow Environmental Observatory,

220 71.3225º N, 156.6231º W), the headwaters of the Sagavanirktok (Sag) River (68.251º N, 149.092º

221 W), and the Teller Road Mile Marker 27 site on the Seward Peninsula (64.73º N, 165.95º W) in

222 Alaska. The simulated hydrological outputs for each site are compared in both column and

223 hillslope scenarios. Column scenarios represent expansive flat regions typical of the Arctic coastal

224 plains dominated by vertical infiltration and heat transport, and hillslope scenarios are

225 representative of the headwater, hilly terrain typical of the more inland permafrost.

226 In hillslope scenarios, hillslopes with northern and southern aspects are considered to investigate

227 physics representation comparisons under the same climate and soil condition (i.e., at a given site)

228 but different solar radiation incidence. Furthermore, hillslopes with both convergent and divergent

229 geometries are included to compare the sensitivity of simulated discharge on process

230 representation. These scenarios can incorporate many types of Arctic systems at the described plot-

231 to-regional scales, but explicitly ignore the effects of microtopography or other local-scale

232 focusing mechanisms such as water tracts or thermo-erosion gullies. The objective is to reach a

233 conclusion on the influence of the three physics representation that can be widely applicable in

234 many Arctic systems.

235 3.1 Field data description

236 For each site, data used in each simulation comprises meteorological forcing datasets for the period

237 2011-2020, averaged wind speed, and soil properties.

238 Meterological forcing datasets are taken from the Daymet version 4 dataset (Thornton et al., 2020),

239 which provides observation-based, daily averaged weather variables through statistical modeling

240 techniques at 1 km spatial resolution (Thornton et al., 2021). Variables that are used in simulations

241 include daily average air temperature (calculated as the mean of Daymet's daily minimum and

242 maximum values), relative humidity (calculated from air temperature and Daymet's vapor

243 pressure), incoming shortwave radiation (W/m^2) (calculated as a product of Daymet's daylit

244 incoming radiation and daylength), and total precipitation (m/s), which is split into snow and rain

245 based upon the air temperature. Figure 1 illustrates the precipitation of rain, snow, and air

246 temperature in the three sites from 2011 to 2020, where the points represent the corresponding

247 averaged values per year. In terms of the forcing conditions, the annual rainfall of the Sag and

248 Teller sites range between 20 and 40 mm/d over the ten years, more than twice the rainfall typical

249 of the Barrow site. In addition, Sag has a significantly larger amount of snow every year that is

250 over double of that at the Teller site and almost five times larger compared to the Barrow site. For

251 the air temperature, Sag and Barrow are similar and colder than Teller by 7-8 degrees. In general,

252 the Barrow site is dry and cold, the Sag site is wet and cold, and the Teller site is wet and warm.
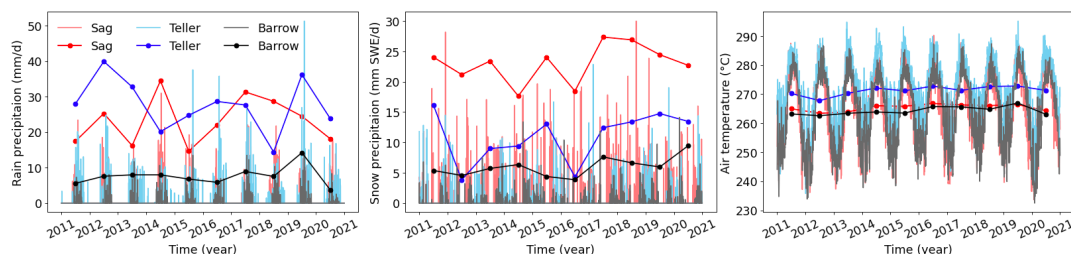
253

254 **Figure 1 Precipitation and air temperature of site Barrow, Sag, and Teller from year 2011 to 2020**

255 In addition to the time series of forcing data from Daymet, we used an average wind speed for

256 each site. For Barrow and Teller, the average wind speed was estimated from the measurement

257 taken by the Next-Generation Ecosystem Experiments (NGEE) Arctic project. At Barrow, the

258 measurement was taken at area A (71.2815º N, 156.6108 º W) at the height of 1.3 meters above

259 surface (Hinzman et al., 2014). At Teller, the measurement at 3.8 m above the surface of a lower

260 level of the watershed (Busey et al., 2017) was used. For Sag, the average wind speed was

261 estimated based on the measurement at the Toolik Lake field site (near to Sag River) at the height

The Cryosphere
Discussions

262   of 3.1 m above surface, which is accessible through the National Ecological Observatory Network

263   (NEON, 2021).

264   The soil properties of Barrow, Sag, and Teller, including porosity, permeability, Van Genuchten

265   parameters, and thermal conductivity parameters, were chosen from previous modeling studies at

266   these sites (Atchley et al., 2015; Jafarov et al., 2018; O'Connor et al., 2020), see (Table 2). Roughly,

267   the soil profile of each site is composed of two materials: the top organic-rich layer comprising

268   mosses, peats, and other organic rich soils measuring approximately 10-30 cm thick, and the

269   principal mineral soil. There is minor difference in thermal conductivity parameters among the

270   three sites, and soil permeability is also at the same order of magnitude. The soil-water

271   characteristic curve (SWCC) of the principal mineral soil of Barrow, Sag, and Teller, shown in

272   Figure 2, indicates that the soil property between Barrow and Teller is relatively similar, while Sag

273   differs from the other two with a relatively flat SWCC.
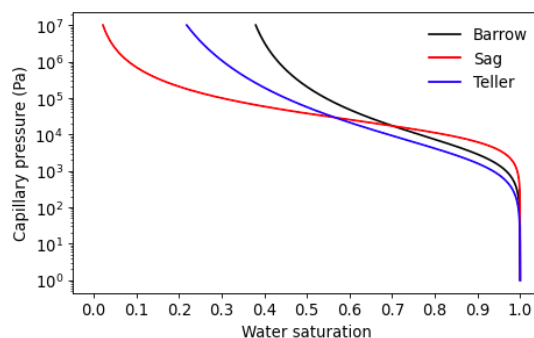
275   **Figure 2 Soil-water characteristic curve (SWCC) of soil in Barrow, Sag, and Teller**

276   Usually, at the hillslope scale, the thickness of organic layers of a watershed varies from the toe-

277   slope, through a steeper mid-hill, up to the flat top. Typically, thicker organic layers may exist at

278   the top and bottom compared to the mid-hillslope. The low thermal conductivity of organic layers

279   can impede the heat transport between the air and the underlying mineral soil, resulting in varying

280   thaw depth (or permafrost table depth) along a hillslope, which has been observed at the site Teller

281   (Jafarov et al., 2018). In this paper, hillslope meshes were constructed following this observation

282   so that the organic layers are thicker at the top and bottom of a hillslope, as described in the next

283   section.

284   **3.2 Mesh design and material properties**

285   The comparison of different physics representations was conducted in both column and hillslope

286   scenarios.

287   The column model was designed as a one-dimensional, 50 m deep domain. The column domain

288   was discretized into 78 cells with gradually increasing cell thickness, starting from 2 cm at the soil

289   surface to 2 m at the bottom of the domain. We assigned different material properties to the cells

290   to represent different soil layers. A column domain is divided into three layers, and the thickness

291   of each layer was designed differently among the three sites according to geological observations

292   (Jan et al., 2020; O'Connor et al., 2020; NGEE-Arctic). Specifically, from top to bottom, the three

293   layers of the Barrow soil column are 2 cm-thick moss, 8 cm-thick peat, and mineral; for Teller, the

294   soil column consists of a 4 cm moss layer, a 22 cm peat layer, and mineral; and the three layers of

295   the Sag soil column are acrotelm, catotelm, with thickness of 10 cm and 14 cm, respectively, and

296   the remainder mineral. The soil properties of each layer at three sites are listed in Table 2.

297   **Table 2 Soil properties of three soil layers of all sites used in this paper**

Site	Barrow			Sag			Teller		
Layers	moss	peat	mineral	acrotelm	catotelm	mineral	moss	peat	mineral
Porosity	0.9	0.876	0.596	0.878	0.796	0.457	0.9	0.55	0.45
Permeability (m^2)	1.7e-11	9.38e-12	6e-13	2.64e-10	9.63e-12	3.98e-13	5e-11	5e-12	2e-13
VG α (Pa^{-1})	2.3e-3	9.5e-4	3.3e-4	7.93e-4	1.75e-4	8.06e-5	2.35e-3	2.93e-4	5.45e-4
VG n	1.38	1.44	1.33	1.405	1.566	1.571	1.38	1.269	1.236
Residual saturation	0.056	0.388	0.334	0.0073	0.0662	0.	0.1	0.	0.1
Thermal conductivity, unfrozen ($Wm^{-1}K^{-1}$)	0.446	0.427	0.788	0.519	0.630	1.309	0.57	0.67	1
Thermal conductivity, dry ($Wm^{-1}K^{-1}$)	0.024	0.025	0.104	0.066	0.086	0.265	0.07	0.07	0.29

298

299   In the hillslope scenario, we designed the mesh based on observations at Teller to represent a

300   generalized, varying-thickness low Arctic hillslope. A hillslope mesh was created first by

301   generating a pseudo-2D surface mesh with 50 cells and then extruding the 2D mesh downward by

302   50 m. The pseudo-2D surface was designed in a trapezoidal shape with a single, variable-width

303   cell in the cross-slope direction to represent convergent/divergent hillslopes, the short and long

304   sides of which are 200 m and 800 m, respectively (see Figure 3). Vertically, from surface

305   downward, the grid size distribution was the same as the column mesh for each site. The domain

306   is also composed of three layers, same as the column, while the numbers of cells representing each

307   soil layer (i.e., soil layer thickness) are different along the hillslope. The thickness distribution of

308   the first two layers of each site is shown in Table 3. The third layer of a hillslope for all sites is the

309   principal mineral soil. Additionally, hillslope meshes with different aspects (i.e., north, south) were
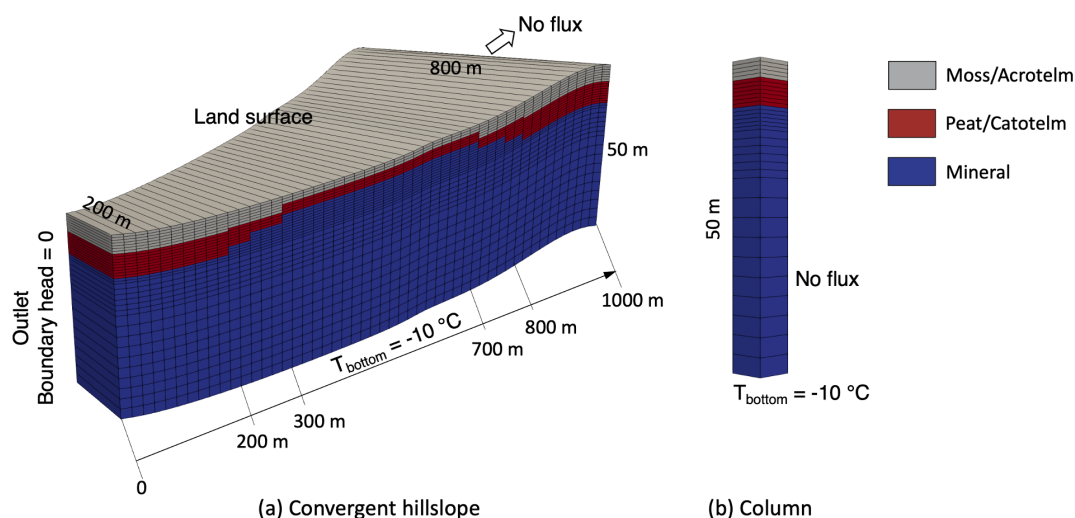
310 also created.

Figure 3 Schematic domain mesh and soil layer partition: (a) example of a convergent hillslope domain, (b) column domain.

311
312
313

314
Table 3 Thickness distribution of the organic layers along hillslope for each site

Site	Horizontal x range (m)	Barrow layer thickness (cm)	Sag layer thickness (cm)	Teller layer thickness (cm)
Layer 1 Moss/Acrotelm	0 ~ 200	2	14	8
	300 ~ 700	2	6	4
	800 ~ 1000	2	14	8
Layer 2 Peat/Catotelm	0 ~ 200	12	18	22
	300 ~ 700	6	8	22
	800 ~ 1000	12	18	22

315 **3.3 Model setup**

not a "process"

316 To study how the representations of the three physical processes (i.e., ice density, cryosuction, and

317 advective heat transport) affect simulated hydrological outputs at different scales and hillslope

318 topography features, and under various forcing and soil conditions, 62 model simulations were

319 conducted, summarized in Table 4. To examine the validity of the assumption of equal density

water

320 between ice and liquid, we included cryosuction and advective heat transport in models. To

321 investigate the role of cryosuction in permafrost modeling, we used different density, while

322 neglecting advective heat transport to decrease the computation cost. Note that neglecting

323 advective heat transport in these runs can reduce the effect of cryosuction on simulation predictions,

324 as cryosuction moves water which would itself advect energy. To compare the difference between

325 neglecting and including heat advection, we used different density expressions for ice and liquid,

326 and included cryosuction. Particularly, in order to understand the impact of advective heat

327 transport on permafrost processes when soil is at its wettest, we designed two extreme cases under

328 the warm, wet conditions of the Teller site in which soil evaporation was artificially reduced.

329 These runs were designed to maximize water flux and therefore maximize the potential for

330 advective heat transport to affect predictions.

331 **Table 4 Ensemble of models designed in this study**

To compare	Site	Scale	Geometry	Aspect	Remark
• $\rho_i \neq \rho_l$, Eq. (1)	Barrow Sag Teller	column	–	–	• heat advection
		hillslope	convergent	north	
				south	
• $\rho_i = \rho_l$, Eq. (2)			divergent	north	• cryosuction
				south	
• Include heat transport	Barrow Sag Teller	column	–	–	• $\rho_i \neq \rho_l$
		hillslope	convergent	north	
				south	
• Neglect heat transport			divergent	north	• cryosuction
				south	
	Extreme case, Teller	hillslope	convergent	north	• reduced evaporation
• Include cryosuction	Barrow Sag Teller	column	–	–	• $\rho_i \neq \rho_l$
		hillslope	convergent	north	
				south	
• Neglect cryosuction			divergent	north	• no heat advection
				south	

332

333 Prior to simulating all cases, two steps of initialization are carried out for each site. First, a column

334 model with a given initial water table depth and above-0 ºC temperature was frozen by setting the

335 bottom temperature at a constant value of -10 ºC until a steady-state frozen soil column is formed.

336 The initial water table depth is chosen to ensure that the frozen column's water table, after

337 accounting for expansion of ice, is just below the soil surface. The pressure and temperature

338 profiles of the frozen column were used as the initial conditions of the second step initialization.

339 Before proceeding, the observed forcing data (period of 2011-2020) was averaged across the years

340 to form a one-year, "typical" forcing year, which was then repeated 10 times. Using this typical

341 forcing data and the solutions of the first step, we solved the column model in a transient solution,

342 calculating an annual cyclic steady-state and obtaining the pressure and temperature fields at the

343 end of the 10th year. The final state was then used as initial condition in formal simulations listed

344 in Table 4. The temperature at bottom was constant at -10 ºC.

345 **3.4 Evaluation metrics**

346   To fully assess the effect of representation of ice density, advective heat transport, and cryosuction

347   in permafrost hydrology modeling, we used root mean squared error (RMSE) and normalized

348   Nash–Sutcliffe efficiency (NNSE) as performance metrics. RMSE has the same dimension with

349   the corresponding variables, which can be used to evaluate the average absolute deviation from a

350   benchmark, defined by:

351    $\text{RMSE} = \sqrt{\frac{\sum_{t=1}^{N}(x_t - y_t)^2}{N}}$ (7)

352   where x_t and y_t are the two modeled datasets to compare from the initial time point ($t = 1$) to the

353   end ($t = N$).

354   NNSE is a normalized dimensionless metric describing the relative relationship between an

355   estimation and a reference, which is oftentimes used for evaluating hydrological models.

356    $\text{NNSE} = 1 / \left(1 + \frac{\sum_{t=1}^{N}(x_t - y_t)^2}{\sum_{t=1}^{N}(x_t - \bar{x})^2}\right)$ (8)

357   where the modeled results x_t (obtained without physics simplification) is considered as the

358   benchmark, and $\bar{x}$ is the mean value of the benchmark. NNSE approaching to 1 indicates perfect

359   correspondence between two observations.

360   In addition, we also used normalized mean absolute error (MAE) to quantify the percentage change

361   of results obtained with simplified physics relative to full physical representations (see Section

362   4.4).

363    $\text{Normalized MAE} = \frac{\sqrt{\sum_{t=1}^{N}|x_t - y_t|/N}}{\text{normalizing reference}} \times 100\%$ (9)

364   Two normalizing references were selected considering different model output variables. For

365   instance, in terms of temperature and saturation which fluctuate between two non-zero values, the

366   annually averaged variation range was chosen as the reference.

367    $\text{Normalizing reference} = \frac{\sum_{\text{year}=1}^{\text{num of years}}(\text{maximum} - \text{minimum})}{\text{number of years}}$

368   For variables with zero as the smallest value, such as evaporation, discharge, and thaw depth, the

369   corresponding average value was selected as the reference.

4 Results

371   This section compares simulated outputs over the period of 2011-2020 for the three physics under

372   different simulating conditions. We focus on the impact on integrated variables, such as

373   evaporation, discharge, averaged thaw depth, and depth-dependent variables, such as temperature,

The Cryosphere
Discussions

374   and total water saturation (ice and liquid). For hillslope models, we chose five surface locations

375   according to the slope geometry to collect simulated data, which were then averaged to obtain a

376   single outcome for each variable of interest.

4.1 Ice density

378   To evaluate the representation of ice density on permafrost process simulation, we compared

379   evaporation, discharge, thaw depth, and total water saturation between simulations using equal and

380   different ice density expressions. Figure 4 and Figure 5 show an example of the comparison under

381   conditions of Sag at the column and hillslope scale, respectively. Results are compared in both time

382   series and correlation.

383   Generally, at both column and hillslope scales, assuming equal density between ice and liquid has

384   minor impacts on evaporation, discharge, and thaw depth over the 10-year simulation, except at a

385   few deviated points as shown in the correlation figures. According to column-based models, the

386   RMSEs of evaporation, discharge, and thaw depth are 0.101 mm/d, 0.001 m^3/d, and 1.648 cm,

387   respectively, one order of magnitude smaller than the corresponding variable values. At the hillslope

388   scale, (see Figure 5) the south-facing divergent hillslope is selected to show modeling comparison

389   on evaporation and thaw depth, in that they are potentially mostly affected when a hillslope has a

390   south orientation and divergent geometry. Likewise, the north-facing convergent hillslope is

391   chosen to compare discharge and water saturation from simulations with different density

392   expressions. Even then, RMSEs of the three variables are 0.064 mm/d, 111.073 m^3/d, and 0.825 cm,

393   respectively, two orders of magnitude smaller than the corresponding variable values at the hillslope

394   scale. Besides, NNSEs of the three variables output from both column and hillslope simulation are

395   over 0.9, approaching 1 especially at the hillslope scale. Therefore, all indicate good performance

396   of equal ice-liquid density assumption in predicting integrated variables and thaw depth. By

397   comparison, the estimation of water saturation is relatively more affected by the density assumption

398   during cold seasons within a year, as shown by Figure 4 (d) and Figure 5 (d). This is reasonable in

399   that when water mainly exists in the form of ice, equal ice-liquid density assumption will

400   overestimate the water content.
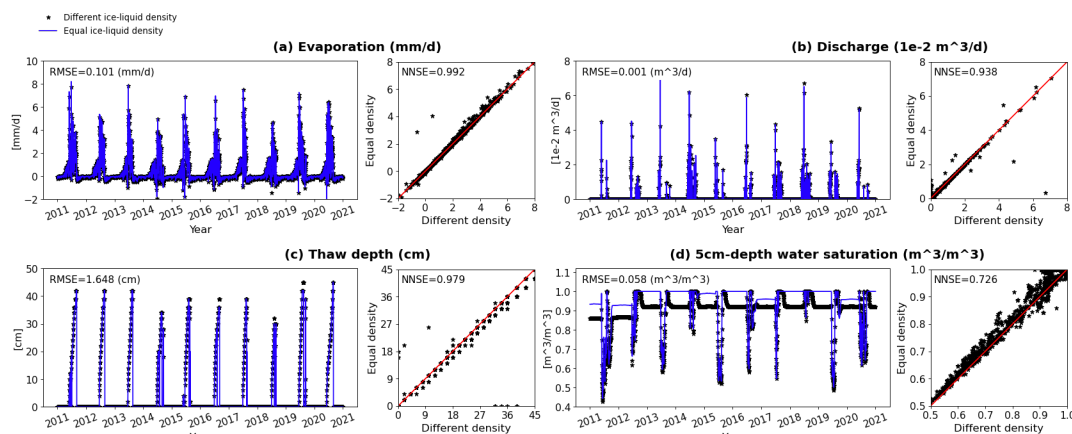
Figure 4 Comparison of column simulations between different and equal ice-liquid density under conditions of Sag, in (a) evaporation, (b) discharge, (c) thaw depth, and (d) water saturation at 5 cm beneath surface from year 2011 to 2020.
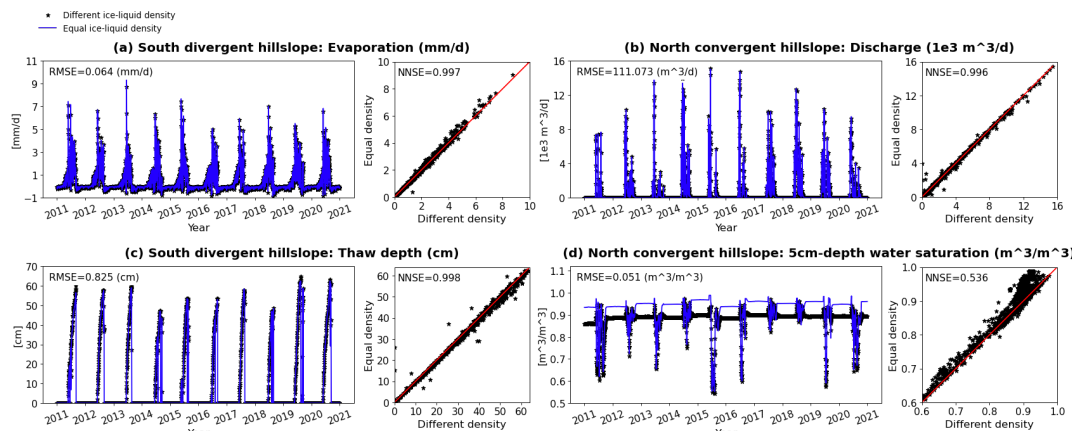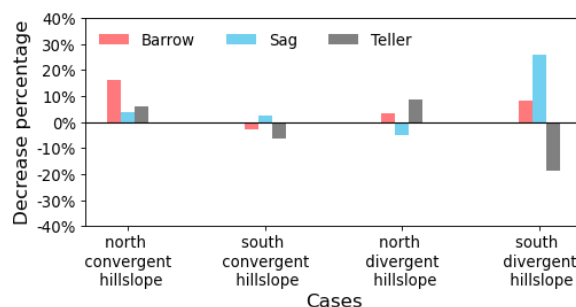

Figure 5 Comparison of hillslope simulations between using different and equal ice-liquid density under conditions of Sag, in (a) evaporation, (b) discharge, (c) thaw depth, and (d) water saturation at 5 cm beneath surface from year 2011 to 2020.

In addition, we investigated how much the assumption of equal ice-liquid density can affect simulation time at the hillslope scale. Using 10-year simulations with real ice density as references, the percentage change of time consumed after applying equal ice-liquid density was calculated and displayed in Figure 6. Overall, under the density assumption, it may take less time (positive percentage), but no more than 25% and on average lower than 10%. However, it may also increase computational time (negative percentage) mainly under wet conditions, such as at Sag and Teller. Thus, given a long-period large-scale modeling of permafrost freezing and thaw processes, there is no consistent conclusion on whether equal ice-liquid density can ease computational cost. It

417 depends on both the weather conditions and soil properties.

Figure 6 Decreased percentage of simulation time under the assumption of equal ice-liquid density compared to the real ice density representation for all hillslope scale simulations.
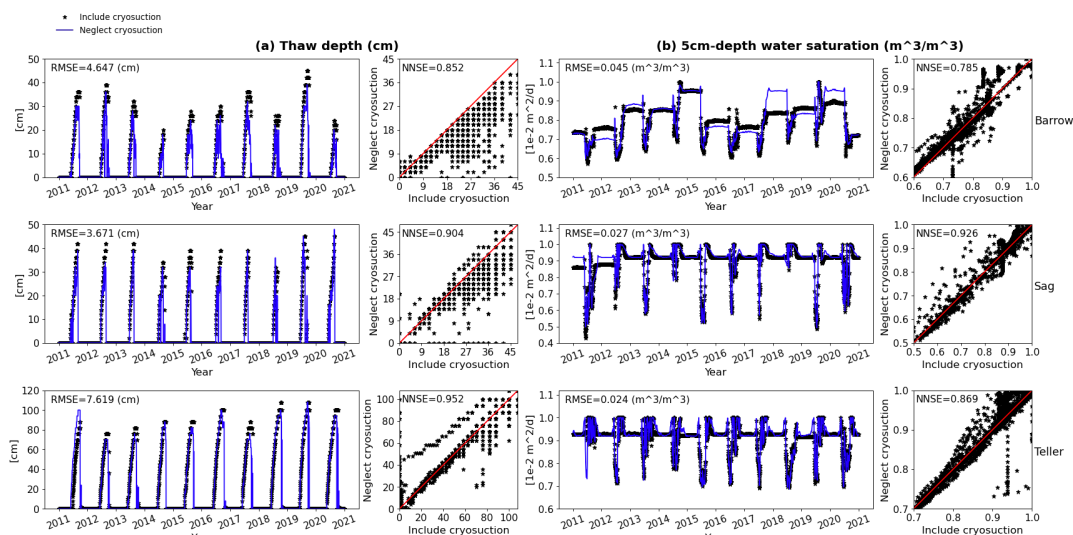
4.2 Cryosuction

To evaluate the effect of cryosuction on permafrost process predictions, we compared evaporation, discharge, thaw depth, total water saturation, and temperature obtained through simulations including and neglecting cryosuction. Figure 7 through Figure 9 illustrate column-scale comparisons of these variables under conditions at the three sites (Barrow, Sag, and Teller). Figure 7 presents the effect of excluding cryosuction on evaporation and discharge. The RMSE of evaporation from the three sites ranges between 0.25 mm/d and 0.35 mm/d, still one order of magnitude smaller than the common evaporation rate. Evaporation NNSEs of the three sites are around 0.9. For discharge, RMSEs are also one order of magnitude smaller than the average, whereas NNSEs fall between 0.6 and 0.9. Generally, cryosuction plays a more important role in predicting discharge compared to evaporation, especially under warm and wet climate conditions, such as Teller.
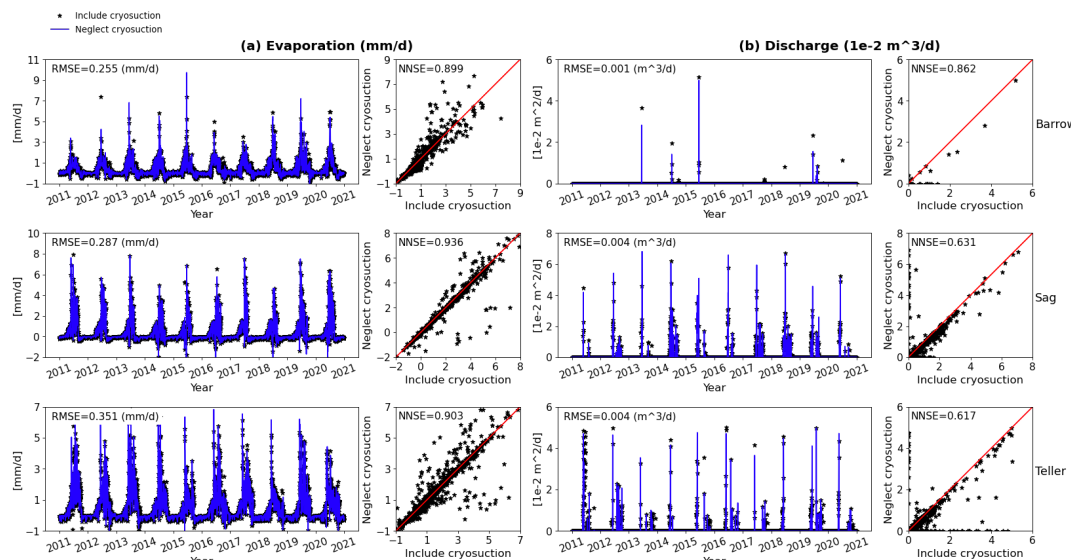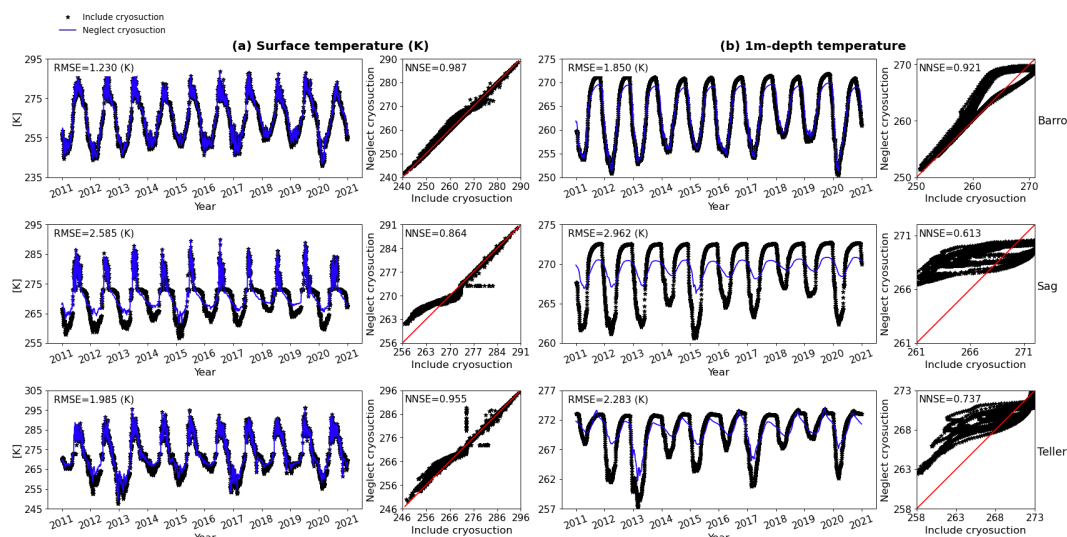
Figure 7 Comparison of column simulations between including and neglecting cryosuction under conditions of Barrow, Sag, and Teller, in (a) evaporation, (b) discharge.

Figure 8 shows the effect of cryosuction on column-scale simulated thaw depth and total water saturation at 5 cm beneath the surface. RMSEs of thaw depth range from 3 cm to 8 cm. Though still one order of magnitude smaller than the average annual thaw depth, the estimation error due to neglecting cryosuction is obvious in summer, especially at areas with cold temperature and low rainfall like Barrow. By comparison, at Teller, where the largest thaw depth is over double that of Barrow and Sag due to its higher temperature, soil cryosuction does not essentially affect thaw depth compared to the other two sites. Similarly, for the total water saturation, at Barrow, the effect of cryosuction is more clearly observed, not only during cold seasons as observed for density representation (section 4.1), but also in summers.

Figure 8 Comparison of column simulations between including and neglecting cryosuction under conditions of Barrow, Sag, and Teller, in (a) thaw depth, (b) water saturation at 5 cm beneath surface.

Finally, we also compared soil temperature obtained from models with or without cryosuction included; see Figure 9. Surface temperature is little affected by cryosuction, except at the Sag site, where the surface temperature is overestimated during winter. At 1 m depth, soil temperature of Barrow is slightly changed in summer due to neglecting cryosuction. At both Sag and Teller, the fluctuation range of temperature at 1 m beneath land surface is underestimated if the cryosuction effect is not considered, especially at Sag, NNSE decreases to 0.6 approximately.

Therefore, from Figure 7 to Figure 9, neglecting cryosuction effect in the column scale simulations has less impact on integrated hydrological variables, but will cause significant difference when estimating thaw depth and location-based variables. The difference among variables varies under different climate conditions. Influence on integrated variables, such as evaporation and discharge, are more obvious under warm and wet conditions (Teller); thaw depth and water saturation are affected more under cold and low-rainfall conditions (Barrow); and soil temperature tends to be influenced greater under cold and high precipitation (rain and snow) conditions (Sag).

Figure 9 Comparison of column simulations between including and neglecting cryosuction under conditions of Barrow, Sag, and Teller, in (a) surface temperature, (b) temperature at 1 m beneath surface.

Neglecting soil cryosuction has a similar impact on hydrological outputs in hillslope scale models. Figure 10 shows the comparison of the variables discussed above under the Sag climate. Evaporation, thaw depth, and temperature are presented based on south-facing divergent hillslope models, while discharge and water saturation are from hillslope models with north-facing convergent geometry. In general, neglecting soil cryosuction has a smaller effect on integrated variables (evaporation and discharge) compared with other pointwise variables. Though thaw depth presents a high NNSE of approximately 0.94, and low RMSE of about 4.5 cm compared to the average, indicating a good match between models considered and excluded cryosuction, the estimation error during summer may reach as high as 10 cm, particularly from 2011 to 2017, as shown in Figure 10 (c). Obvious errors in water saturation and temperature, similar with column-scale models, occur almost annually with respect to extrema during winter and summer. Overall, compared to column-scale models, differences in evaporation, discharge, thaw depth, and surface temperature due to neglecting cryosuction effect are relatively reduced at the hillslope scale if comparing NNSEs (Table 5). Localized subsurface variables, such as water saturation and 1m-depth soil temperature, show increased errors from column to hillslope scale models, which is primarily caused by lateral flux exchange captured by hillslope modeling.
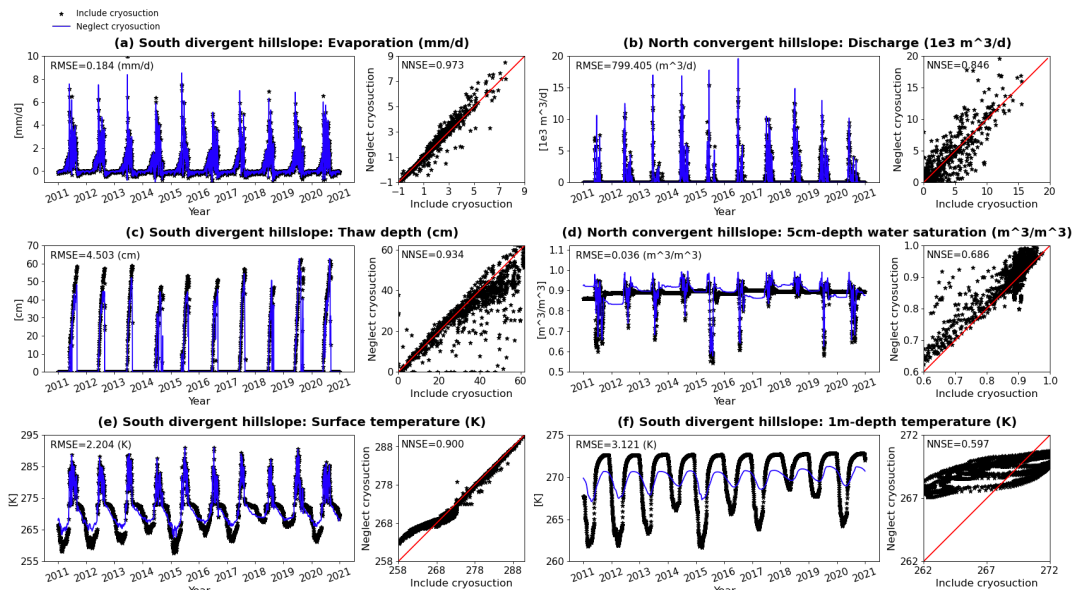
20

479
480 **Figure 10 Comparison of hillslope simulations between including and neglecting cryosuction under conditions**
481 **of Sag, in (a) evaporation, (b) discharge, (c) thaw depth, (d) water saturation at 5 cm beneath surface, (e)**
482 **surface temperature, (f) temperature at 1 m beneath surface.**

483 **Table 5 NNSE of outputs from column and hillslope models under conditions of Sag**
484 **shown in Figure 7 through Figure 10**

Scale	Evaporation (mm/d)	Discharge (m³/d)	Thaw depth (cm)	5cm-depth water saturation (-)	Surface temperature (K)	1m-depth temperature (K)
Column	0.936	0.631	0.904	0.926	0.864	0.613
Hillslope	0.973	0.846	0.934	0.686	0.900	0.597

485

486 **4.3 Advective heat transport**

487 This section evaluates the performance of advective heat transport in modeling permafrost process.

488 As above, we investigated the influence of neglecting heat advection on evaporation, discharge,

489 thaw depth, total water saturation, and temperature. Overall, heat advection does not play a vital

490 role in a normal Arctic system after comparing all hydrological outputs from models with different

491 heat transport representations. Comparisons based on column-scale and hillslope-scale models are

492 not shown here (see Supplement); instead, the extreme case under conditions of Teller is presented

493 (Figure 11). Teller is abundant in rainfall over the period of 2011-2020 (Figure 1). In the extreme

494 case, evaporation was reduced factitiously to almost a quarter of the original value (see Figure 7

495 (a) at Teller and Figure 11 (a)) for the purpose of increasing water flow rates. For instance,

496 discharge has quadrupled after adjusting evaporation by comparing Figure 11 (b) and Figure 7 (b)

497   at Teller. This specific scenario is chosen to maximize the potential effect of advective heat

498   transport in a hillslope-scale Arctic system. Figure 11 illustrates comparisons on all outputs

499   mentioned above from hillslope models without heat advection and with full thermal

500   representation. Apparently, all RMSEs are extremely small, at least two orders of magnitude lower

501   than the corresponding variable average. Almost all NNSEs are approximately one, even for thaw

502   depth, localized water saturation, and temperature. Therefore, for most Arctic systems at this scale,

503   it is reasonable to neglect advective heat transport.

? much too general.
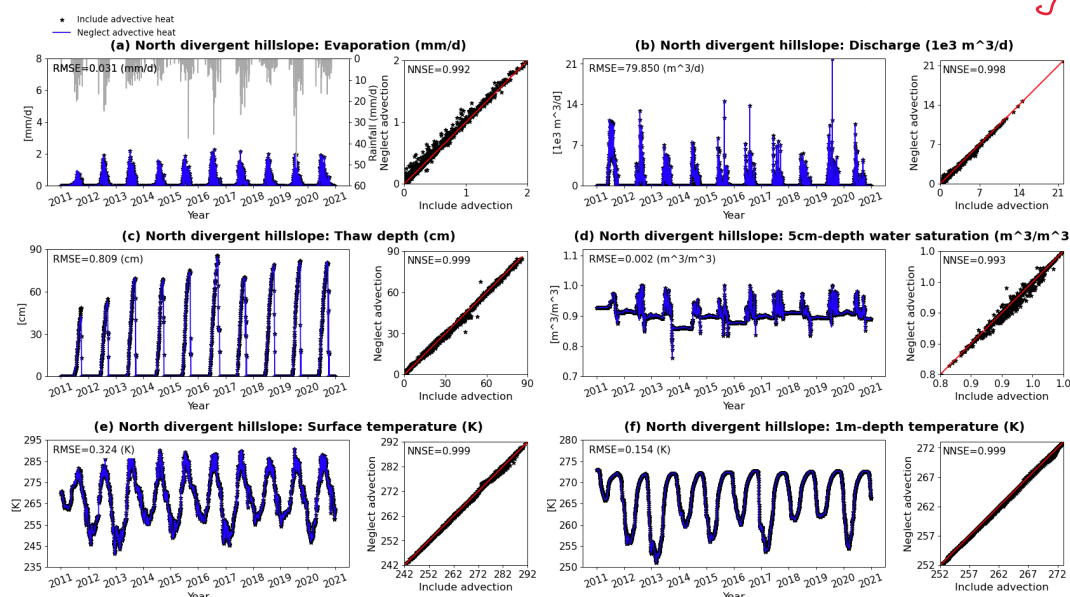
Figure 11 Comparison of hillslope simulations between including and neglecting advective heat transport under extreme conditions of Teller, in (a) evaporation, (b) discharge, (c) thaw depth, (d) water saturation at 5 cm beneath surface, (e) surface temperature, (f) temperature at 1 m beneath surface.

508   In addition to simulated results, we also compared simulation times in percentage change between

509   hillslope models neglecting and including heat advection. ATS uses Algebraic Multigrid method

510   as preconditioner for solving, which has a relatively deficient performance in dealing with

511   hyperbolic equations. Thus, incorporating advective heat transport will aggravate computational

512   cost, particularly in case of both large spatial and temporal scale. Figure 12 shows the relative

513   percentage reduction in computational time for 10-year simulations after excluding heat advection

514   in both surface and subsurface thermal flux. It drops by 70% ~ 80% under wet conditions (e.g.,

515   Sag and Teller) and 40% ~ 60% under dry conditions (e.g., Barrow). Hence, neglecting advective

516   heat transport considerably improves the performance of large spatial-temporal permafrost

*Computational cost should be irrelevant.
If advective heat transport is relevant, it needs to be included.*

517 hydrology simulations.
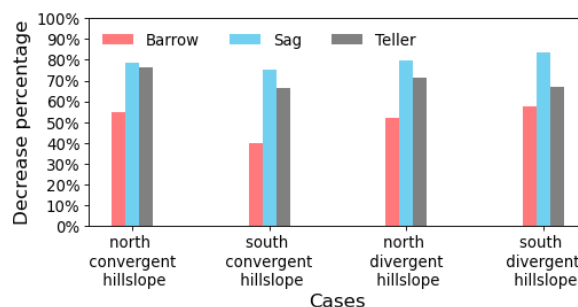
518
519 **Figure 12 Decreased percentage of simulation time after neglecting heat advection compared to full thermal**
520 **representation for all hillslope scale simulations.**

521 **4.4 Comprehensive comparison**

522 In the above three sections, we discussed time-series simulation comparisons. This section will

523 analyze the effect of equal ice-liquid density, neglecting cryosuction, and neglecting heat

524 advection on permafrost modeling outputs from holistic, average perspectives.

525 First, we extracted NNSEs of all variables obtained from all comparing models for qualitative

526 analysis. Table 6 shows an example based on column-scale models under conditions of three

527 different sites. Red numbers highlight the obviously reduced NNSEs of one or two processes

528 among the three for each variable. Overall, neglecting advective heat transport has the least

529 influence on model outputs. Equal ice-liquid density primarily affects saturation and has less effect

530 on other variables. Excluding soil cryosuction makes the greatest impact on almost all variables,

531 especially in a relatively wet environment. Among the variables, evaporation and surface

532 temperature are less affected by the three physical process representations, while location-based

533 water saturation is most affected.

534 **Table 6 A summary of NNSEs of variables obtained through column model comparison**

Variables	Barrow			Sag			Teller		
	Heat advection	*Ice density*	*Cryosuction*	*Heat advection*	*Ice density*	*Cryosuction*	*Heat advection*	*Ice density*	*Cryosuction*
Evaporation	0.9971	0.9942	0.8991	0.9926	0.9917	0.9365	0.9989	0.9958	0.9033
Discharge	0.9235	0.6282	0.8615	0.9962	0.9377	0.6305	0.9854	0.9874	0.6175
Thaw depth	0.9970	0.9961	0.8517	0.9910	0.9791	0.9036	0.9969	0.9887	0.9524
5cm-depth s_w	0.9959	0.9335	0.7851	0.9916	0.7260	0.9260	0.9979	0.5618	0.8690
40cm-depth s_w	0.9932	0.0221	0.2130	0.9951	0.0622	0.3111	0.9990	0.2807	0.8498
Surface T	0.9999	0.9999	0.9871	0.9993	0.9990	0.8642	0.9999	0.9996	0.9554
1m-depth T	0.9999	0.9999	0.9207	0.9997	0.9996	0.6127	0.9997	0.9991	0.7366

Do you really need 4 digits? 3 seems enough.

The Cryosphere
Discussions

physical processes,

535   * s_w and T in Table 6 are water saturation and temperature, respectively.

536   Furthermore, to compare across the physics *quantitively*, we calculated the mean absolute error

537   (MAE) for each variable of interest over the simulation period of 2011-2020. For evaporation,

538   discharge, and thaw depth, the MAEs are normalized by the corresponding variable average

539   (numbers in Figure 13 (a)); for water saturation and temperature, the MAEs are normalized by

540   their average annual fluctuation range (numbers in Figure 13 (b)). All normalized MAEs are

541   presented in percentage, displayed in Figure 13 according to column- and hillslope-scale (e.g.,

542   south-facing convergent hillslope) models under three different climate conditions. Hillslope-scale

543   model output under conditions of Barrow is not shown in that flat land occupies a majority of the

544   area. A larger normalized MAE percentage indicates greater impact on the variable resulted from

545   a physical process.

546   From the perspective of 10-year average, in general, each physical process of Arctic systems

547   discussed in this paper presents a similar impact on variables between column and hillslope scales.

548   Under climate and soil conditions of three different sites, neglecting cryosuction in permafrost

549   modeling leads to the greatest influence on hydrological prediction amongst the three physical

550   assumptions. As seen in Figure 13 (a), it will result in 10% ~ 20% deviation in evaporation, 50%

551   ~ 60% in discharge, and 10% ~ 30% in thaw depth. Evaporation is the least affected among the

552   three variables. Discharge is more affected in regions with abundant rainfall (Teller), while in

553   regions with less precipitation, evaporation and thaw depth are relatively affected (Barrow). By

554   comparison, assuming equal ice-liquid density and neglecting advective heat transport may only

555   cause 10% and 5% or even much lower error, respectively, in reference to the annual average of a

556   variable. *Specifically,* Specially in Barrow, models utilizing the same ice and liquid densities and ignoring

557   advective heat *transport* seem to make an obvious impact on discharge, whereas this also results from its

558   extremely low discharge (Figure 7 (b)).

559   Figure 13 (b) illustrates the normalized MAEs of water saturation at 5 cm beneath surface, as well

560   as temperature at surface and 1 m depth. The assumption of equal ice-liquid density primarily

561   affects the estimation of *the* water saturation profile, *which* it can lead to about 5% ~ 15% error relative to

562   the annual change range, and the error percentage tends to slightly decrease when applying

563   hillslope-scale models due to the inclusion of lateral flow. Apart from this, neglecting soil

564   cryosuction still makes the largest impact. Surface temperature is the least affected variable among

565   all these model outputs even if cryosuction is not included in modeling. However, at 1 m depth,

566 error can increase to 10% ~ 30% by simulation without cryosuction representation.
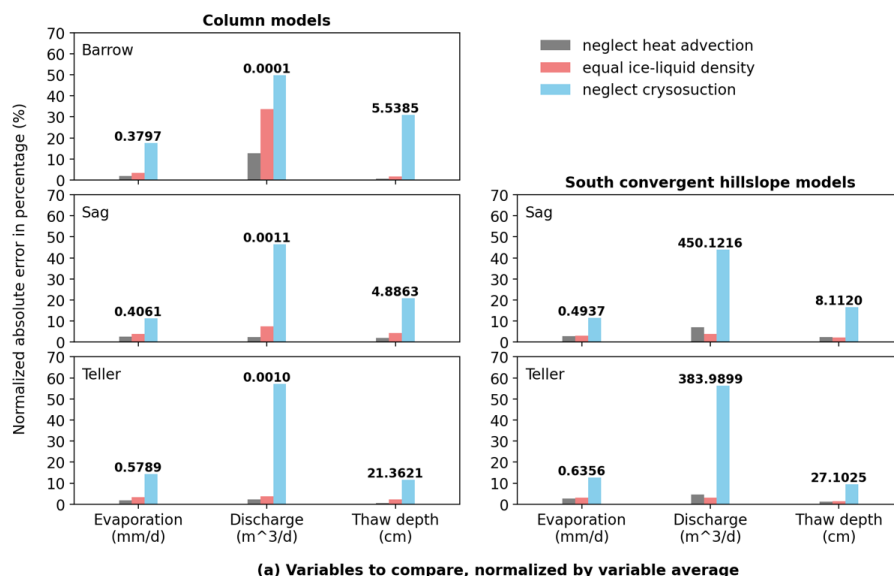
(a) Variables to compare, normalized by variable average
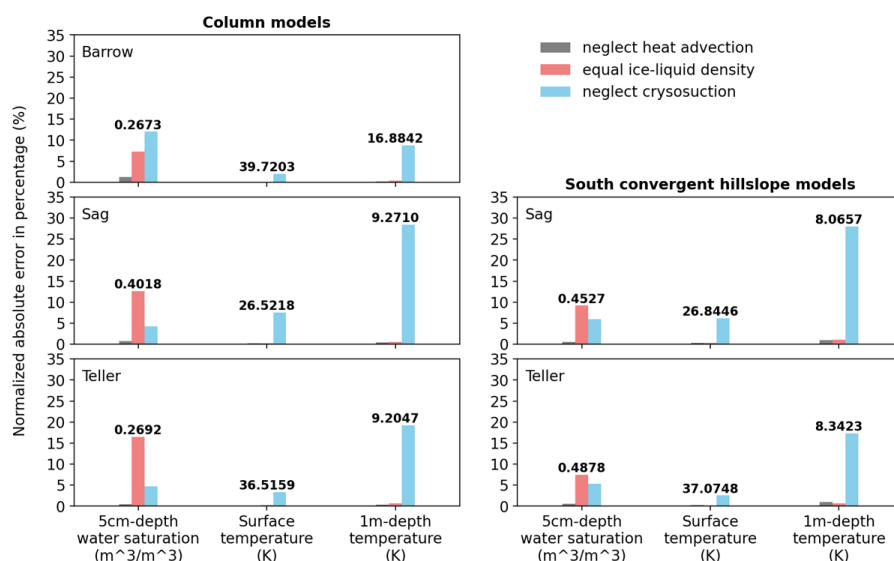
(b) Variables to compare, normalized by average annual fluctuation of variables

Figure 13 Normalized average absolute error of variables over the period of 2011-2020, compared among three physical assumptions at column and hillslope scales. Variables: (a) evaporation, discharge, and thaw depth, numbers in figures are the average values of the corresponding variables; (b) water saturation, and temperature, numbers in figures are the average annual fluctuation range of each variable.

574 **5 Conclusion**

575 Simplification of Arctic process representation is an essential consideration when developing

576 process-rich models for thermal permafrost hydrology. There are three subsurface processes that

577 are commonly described in a simplified approach for many Arctic tundra models: (i) ice is

578 prescribed the same density as liquid water; (ii) the effect of soil cryosuction is neglected; (iii)

579 advective heat transport is neglected. Here we investigated the influence of these simplified

580 representations on modeling field-scale permafrost hydrology.

[handwritten margin note: these are not cast as "processes" here, They are here cast as "process simplification"]

581 To do this, we conducted an ensemble of simulations using the Advanced Terrestrial Simulator

582 (ATS v1.2) to evaluate the impact of the above three process simplifications on field-scale

583 predictions. The ensemble of simulations consisted of 62 numerical experiments considering

584 various conditions, including different climate conditions and soil properties at three sites of

585 Alaska, and different model scale conceptualizations. For evaluation, we compared integrated

586 variables (evaporation, discharge), averaged thaw depth, and pointwise variables (temperature,

587 total water saturation), among different models to access the deviation of applying a simplified

588 modeling assumption. The main conclusions of this study are summarized as follows:

1) Excluding soil cryosuction in permafrost models can cause significant bias in most
   hydrological variables. ~~Especially, according to~~ *[handwritten: In particular, under the assumed conditions of]* this study, the average deviation in
   evaporation, discharge, and thaw depth may reach 10% ~ 20%, 50% ~ 60%, and 10% ~
   30%, respectively, relative to the corresponding annual average values. The prediction
   error for discharge may grow if rainfall rates increase. In the case of pointwise variables,
   the error in temperature increases from a small amount at the surface up to 10% ~ 30% at
   1 m beneath surface. The prediction of subsurface temperature and water saturation is
   especially affected when considering hillslope scale models. Therefore, soil cryosuction
   should be included when modeling permafrost change.

2) Assuming equal ice-liquid density will not result in especially large deviations when
   predicting most of the hydrological variables, particularly at hillslope scales. It primarily
   affects the prediction of *[handwritten: the]* soil water saturation profile and can cause 5% ~ 15% error relative
   to the annual saturation fluctuation range. This difference may have consequences for the
   carbon cycle with regards to the production of methane versus carbon dioxide. Assigning
   liquid water density for ice may reduce computational time to a small extent in ATS,
   dependent on simulating conditions and spatial and temporal scales.

3) For a general Arctic tundra system, the prediction error in most variables after neglecting

The Cryosphere
Discussions

[Handwritten margin note: All results were focussed on the errors in making these simplifications, more discussion would help in identifying why some were more sensitive than others, i.e. need to provide more insight into the role of the physical processes. Also - no spatial results shown of 3D model?]

606   advective heat transport is less than 5%, or even much lower. In the case of ATS, the

607   simulation time cost for hillslope-scale models can decrease by 40% to 80% under

608   conditions in this study. Ignoring heat advection in the absence of local, flow-focusing

609   mechanisms, such as thermo-erosion gullies, seems a reasonable decision.

610 Through the comparison of permafrost hydrological outputs obtained from ensemble model setups

611 targeted at field scale, we confirm the importance and necessity of including soil cryosuction effect

612 in predicting permafrost changes, and valid application of equal ice-liquid density and neglecting

613 advective heat transport for a general Arctic system. The latter two may also ease computational

614 cost dependent upon simulation conditions. We expect that this study can contribute to the

615 development of permafrost hydrology models, as well as better selection of physical process

616 representations for modelers.

Code availability

617

618 Advanced Terrestrial Simulator (ATS) is an open-source code for solving ecosystem-based,

619 integrated, distributed hydrology, and available at https://github.com/amanzi/ats. Simulations were

620 conducted using version 1.2 (Coon et al., 2021).

Data availability

621

622 Data sources of wind speed are cited in the text. The raw forcing data acquired from Daymet, the

623 processed forcing data used for simulation, and simulation output data are available through

624 https://github.com/gaobhub/data_for_paper_model_comparison.

Author contributions

625

626 Bo Gao did some revision of the code to add options for process representations, designed

627 numerical experiments and setup models, did data analysis and interpretation, drafted and revised

628 the article. Ethan T. Coon implemented the code in which the study was done, conceptualized the

629 study, helped debug the runs, and helped draft and revise the article.

Competing interests

630

631 The authors declare that they have no conflict of interest.

638 **References**

639   Abolt, C. J., Young, M. H., Atchley, A. L., Harp, D. R., and Coon, E. T.: Feedbacks Between
640   Surface Deformation and Permafrost Degradation in Ice Wedge Polygons, Arctic Coastal Plain,
641   Alaska, J. Geophys. Res. Earth Surf., 125, e2019JF005349,
642   https://doi.org/10.1029/2019JF005349, 2020.

643   Atchley, A. L., Painter, S. L., Harp, D. R., Coon, E. T., Wilson, C. J., Liljedahl, A. K., and
644   Romanovsky, V. E.: Using field observations to inform thermal hydrology models of permafrost
645   dynamics with ATS (v0.83), Geosci. Model Dev., 8, 2701–2722, https://doi.org/10.5194/gmd-8-
646   2701-2015, 2015.

647   Berteaux, D., Gauthier, G., Domine, F., Ims, R. A., Lamoureux, S. F., Lévesque, E., and Yoccoz,
648   N.: Effects of changing permafrost and snow conditions on tundra wildlife: critical places and
649   times, Arct. Sci., 3, 65–90, https://doi.org/10.1139/as-2016-0023, 2017.

650   Bui, M. T., Lu, J., and Nie, L.: A Review of Hydrological Models Applied in the Permafrost-
651   Dominated Arctic Region, Geosciences, 10, 401, https://doi.org/10.3390/geosciences10100401,
652   2020.

653   Busey, B., Bolton, B., Wilson, C., and Cohen, L.: Surface Meteorology at Teller Site Stations,
654   Seward Peninsula, Alaska, Ongoing from 2016, Next Generation Ecosystem Experiments Arctic
655   Data Collection, Oak Ridge National Laboratory, U.S. Department of Energy, Oak Ridge,
656   Tennessee, USA. Dataset accessed on October 10, 2021 at https://doi.org/10.5440/1437633,
657   2017.

658   Chen, L., Fortier, D., McKenzie, J. M., and Sliger, M.: Impact of heat advection on the thermal
659   regime of roads built on permafrost, Hydrol. Process., 34, 1647–1664,
660   https://doi.org/10.1002/hyp.13688, 2020.

661   Cheng, G. and Wu, T.: Responses of permafrost to climate change and their environmental
662   significance, Qinghai-Tibet Plateau, J. Geophys. Res. Earth Surf., 112,
663   https://doi.org/10.1029/2006JF000631, 2007.

664   Coon, E. T., David Moulton, J., and Painter, S. L.: Managing complexity in simulations of land
665   surface and near-surface processes, Environ. Model. Softw., 78, 134–149,
666   https://doi.org/10.1016/j.envsoft.2015.12.017, 2016.

667   Coon, E. T., Moulton, J. D., Kikinzon, E., Berndt, M., Manzini, G., Garimella, R., Lipnikov, K.,
668   and Painter, S. L.: Coupling surface flow and subsurface flow in complex soil structures using

669   mimetic finite differences, Adv. Water Resour., 144, 103701,
670   https://doi.org/10.1016/j.advwatres.2020.103701, 2020.

671   Coon, E. T., Berndt, M., Jan, A., Svyatsky, D., Atchley, A. L., Kikinzon, E., Harp, D. R.,
672   Manzini, G., Shelef, E., Lipnikov, K., Garimella, R., Xu, C., Moulton, D., Karra, S., Painter, S.
673   L., Jafarov, E., and Molins, S.: Advanced Terrestrial Simulator. U.S. Department of Energy,
674   USA. Version 1.2. DOI: 10.11578/dc.20190911.1, 2021.

675   Dall'Amico, M., Endrizzi, S., Gruber, S., and Rigon, R.: A robust and energy-conserving model
676   of freezing variably-saturated soil, The Cryosphere, 5, 469–484, https://doi.org/10.5194/tc-5-
677   469-2011, 2011.

678   Dearborn, K. D., Wallace, C. A., Patankar, R., and Baltzer, J. L.: Permafrost thaw in boreal
679   peatlands is rapidly altering forest community composition, J. Ecol., 109, 1452–1467,
680   https://doi.org/10.1111/1365-2745.13569, 2021.

681   Devoie, É. G. and Craig, J. R.: A Semianalytical Interface Model of Soil Freeze/Thaw and
682   Permafrost Evolution, Water Resour. Res., 56, e2020WR027638,
683   https://doi.org/10.1029/2020WR027638, 2020.

684   Endrizzi, S., Gruber, S., Dall'Amico, M., and Rigon, R.: GEOtop 2.0: simulating the combined
685   energy and water balance at and below the land surface accounting for soil freezing, snow cover
686   and terrain effects, Geosci. Model Dev., 7, 2831–2857, https://doi.org/10.5194/gmd-7-2831-
687   2014, 2014.

688   Fortier, D., Allard, M., and Shur, Y.: Observation of rapid drainage system development by
689   thermal erosion of ice wedges on Bylot Island, Canadian Arctic Archipelago, Permafr. Periglac.
690   Process., 18, 229–243, https://doi.org/10.1002/ppp.595, 2007.

691   Godin, E., Fortier, D., and Coulombe, S.: Effects of thermo-erosion gullying on hydrologic flow
692   networks, discharge and soil loss, Environ. Res. Lett., 9, 105010, https://doi.org/10.1088/1748-
693   9326/9/10/105010, 2014.

694   Gottardi, G. and Venutelli, M.: A control-volume finite-element model for two-dimensional
695   overland flow, Adv. Water Resour., 16, 277–284, https://doi.org/10.1016/0309-1708(93)90019-
696   C, 1993.

697   Harp, D. R., Zlotnik, V., Abolt, C. J., Busey, B., Avendaño, S. T., Newman, B. D., Atchley, A.
698   L., Jafarov, E., Wilson, C. J., and Bennett, K. E.: New insights into the drainage of inundated
699   ice-wedge polygons using fundamental hydrologic principles, The Cryosphere, 15, 4005–4029,
700   https://doi.org/10.5194/tc-15-4005-2021, 2021.

701   Hinzman, L., Busey, B., Cable, W., and Romanovsky, V.: Surface Meteorology, Utqiagvik
702   (Barrow), Alaska, Area A, B, C and D, Ongoing from 2012, Next Generation Ecosystem
703   Experiments Arctic Data Collection, Oak Ridge National Laboratory, U.S. Department of
704   Energy, Oak Ridge, Tennessee, USA. Dataset accessed on October 10, 2021 at
705   https://doi.org/10.5440/1164893, 2014.

706   Hjort, J., Karjalainen, O., Aalto, J., Westermann, S., Romanovsky, V. E., Nelson, F. E.,
707   Etzelmüller, B., and Luoto, M.: Degrading permafrost puts Arctic infrastructure at risk by mid-
708   century, Nat. Commun., 9, 5147, https://doi.org/10.1038/s41467-018-07557-4, 2018.

709   Hugelius, G., Strauss, J., Zubrzycki, S., Harden, J. W., Schuur, E. a. G., Ping, C.-L.,

710 Schirrmeister, L., Grosse, G., Michaelson, G. J., Koven, C. D., O'Donnell, J. A., Elberling, B.,
711 Mishra, U., Camill, P., Yu, Z., Palmtag, J., and Kuhry, P.: Estimated stocks of circumpolar
712 permafrost carbon with quantified uncertainty ranges and identified data gaps, Biogeosciences,
713 11, 6573–6593, https://doi.org/10.5194/bg-11-6573-2014, 2014.

714 Jafarov, E. E., Coon, E. T., Harp, D. R., Wilson, C. J., Painter, S. L., Atchley, A. L., and
715 Romanovsky, V. E.: Modeling the role of preferential snow accumulation in through talik
716 development and hillslope groundwater flow in a transitional permafrost landscape, Environ.
717 Res. Lett., 13, 105006, https://doi.org/10.1088/1748-9326/aadd30, 2018.

718 Jan, A., Coon, E. T., Painter, S. L., Garimella, R., and Moulton, J. D.: An intermediate-scale
719 model for thermal hydrology in low-relief permafrost-affected landscapes, Comput. Geosci., 22,
720 163–177, https://doi.org/10.1007/s10596-017-9679-3, 2018.

721 Jan, A., Coon, E. T., and Painter, S. L.: Evaluating integrated surface/subsurface permafrost
722 thermal hydrology models in ATS (v0.88) against observations from a polygonal tundra site,
723 Geosci. Model Dev., 13, 2259–2276, https://doi.org/10.5194/gmd-13-2259-2020, 2020.

724 Jorgenson, M. T., Racine, C. H., Walters, J. C., and Osterkamp, T. E.: Permafrost Degradation
725 and Ecological Changes Associated with a WarmingClimate in Central Alaska, Clim. Change,
726 48, 551–579, https://doi.org/10.1023/A:1005667424292, 2001.

727 Karra, S., Painter, S. L., and Lichtner, P. C.: Three-phase numerical model for subsurface
728 hydrology in permafrost-affected regions (PFLOTRAN-ICE v1.0), The Cryosphere, 8, 1935–
729 1950, https://doi.org/10.5194/tc-8-1935-2014, 2014.

730 Kurylyk, B. L. and Watanabe, K.: The mathematical representation of freezing and thawing
731 processes in variably-saturated, non-deformable soils, Adv. Water Resour., 60, 160–177,
732 https://doi.org/10.1016/j.advwatres.2013.07.016, 2013.

733 Kurylyk, B. L., MacQuarrie, K. T. B., and McKenzie, J. M.: Climate change impacts on
734 groundwater and soil temperatures in cold and temperate regions: Implications, mathematical
735 theory, and emerging simulation tools, Earth-Sci. Rev., 138, 313–334,
736 https://doi.org/10.1016/j.earscirev.2014.06.006, 2014.

737 Luethi, R., Phillips, M., and Lehning, M.: Estimating Non-Conductive Heat Flow Leading to
738 Intra-Permafrost Talik Formation at the Ritigraben Rock Glacier (Western Swiss Alps), Permafr.
739 Periglac. Process., 28, 183–194, https://doi.org/10.1002/ppp.1911, 2017.

740 McKenzie, J. M. and Voss, C. I.: Permafrost thaw in a nested groundwater-flow system,
741 Hydrogeol. J., 21, 299–316, https://doi.org/10.1007/s10040-012-0942-3, 2013.

742 McKenzie, J. M., Voss, C. I., and Siegel, D. I.: Groundwater flow with energy transport and
743 water–ice phase change: numerical simulations, benchmarks, and application to freezing in peat
744 bogs, Adv. Water Resour., 30, 966–983, https://doi.org/10.1016/j.advwatres.2006.08.008, 2007.

745 NEON (National Ecological Observatory Network): 2D wind speed and direction
746 (DP1.00001.001): RELEASE-2021, https://doi.org/10.48443/s9ya-zc81, 2021. Dataset accessed
747 from https://data.neonscience.org on October 10, 2021.

748 Nixon, J. F.: The Role of Convective Heat Transport in the Thawing of Frozen Soils, Can.
749 Geotech. J., 12, 425–429, https://doi.org/10.1139/t75-046, 1975.

750 Noh, J.-H., Lee, S.-R., and Park, H.: Prediction of cryo-SWCC during freezing based on pore-

751   size distribution, Int. J. Geomech., 12, 428–438, https://doi.org/10.1061/(ASCE)GM.1943-
752   5622.0000134, 2012.

753   O'Connor, M. T., Cardenas, M. B., Ferencz, S. B., Wu, Y., Neilson, B. T., Chen, J., and Kling,
754   G. W.: Empirical Models for Predicting Water and Heat Flow Properties of Permafrost Soils,
755   Geophys. Res. Lett., 47, e2020GL087646, https://doi.org/10.1029/2020GL087646, 2020.

756   Painter, S. L.: Three-phase numerical model of water migration in partially frozen geological
757   media: model formulation, validation, and applications, Comput. Geosci., 15, 69–85,
758   https://doi.org/10.1007/s10596-010-9197-z, 2011.

759   Painter, S. L. and Karra, S.: Constitutive Model for Unfrozen Water Content in Subfreezing
760   Unsaturated Soils, Vadose Zone J., 13, vzj2013.04.0071,
761   https://doi.org/10.2136/vzj2013.04.0071, 2014.

762   Painter, S. L., Coon, E. T., Atchley, A. L., Berndt, M., Garimella, R., Moulton, J. D., Svyatskiy,
763   D., and Wilson, C. J.: Integrated surface/subsurface permafrost thermal hydrology: Model
764   formulation and proof-of-concept simulations: integrated pemafrost thermal hydrology, Water
765   Resour. Res., 52, 6062–6077, https://doi.org/10.1002/2015WR018427, 2016.

766   Riseborough, D., Shiklomanov, N., Etzelmüller, B., Gruber, S., and Marchenko, S.: Recent
767   advances in permafrost modelling, Permafr. Periglac. Process., 19, 137–156,
768   https://doi.org/10.1002/ppp.615, 2008.

769   Rowland, J. C., Travis, B. J., and Wilson, C. J.: The role of advective heat transport in talik
770   development beneath lakes and ponds in discontinuous permafrost, Geophys. Res. Lett., 38,
771   https://doi.org/10.1029/2011GL048497, 2011.

772   Sjöberg, Y., Coon, E., K. Sannel, A. B., Pannetier, R., Harp, D., Frampton, A., Painter, S. L., and
773   Lyon, S. W.: Thermal effects of groundwater flow through subarctic fens: A case study based on
774   field observations and numerical modeling, Water Resour. Res., 52, 1591–1606,
775   https://doi.org/10.1002/2015WR017571, 2016.

776   Stuurop, J. C., van der Zee, S. E. A. T. M., Voss, C. I., and French, H. K.: Simulating water and
777   heat transport with freezing and cryosuction in unsaturated soil: Comparing an empirical, semi-
778   empirical and physically-based approach, Adv. Water Resour., 149, 103846,
779   https://doi.org/10.1016/j.advwatres.2021.103846, 2021.

780   Sugimoto, A., Yanagisawa, N., Naito, D., Fujita, N., and Maximov, T. C.: Importance of
781   permafrost as a source of water for plants in east Siberian taiga, Ecol. Res., 17, 493–503,
782   https://doi.org/10.1046/j.1440-1703.2002.00506.x, 2002.

783   Tesi, T., Muschitiello, F., Smittenberg, R. H., Jakobsson, M., Vonk, J. E., Hill, P., Andersson,
784   A., Kirchner, N., Noormets, R., Dudarev, O., Semiletov, I., and Gustafsson, Ö.: Massive
785   remobilization of permafrost carbon during post-glacial warming, Nat. Commun., 7, 13653,
786   https://doi.org/10.1038/ncomms13653, 2016.

787   Thornton, M. M., Wei, Y., Thornton, P. E., Shrestha, R., Kao, S., and Wilson, B. E.: Daymet:
788   Station-Level Inputs and Cross-Validation Result for North America, Version 4,
789   https://doi.org/10.3334/ORNLDAAC/1850, 2020.

790   Thornton, P. E., Shrestha, R., Thornton, M., Kao, S.-C., Wei, Y., and Wilson, B. E.: Gridded
791   daily weather data for North America with comprehensive uncertainty quantification, Sci. Data,

792   8, 190, https://doi.org/10.1038/s41597-021-00973-0, 2021.

793   Van Genuchten, M. T.: A Closed-form Equation for Predicting the Hydraulic Conductivity of
794   Unsaturated Soils, Soil Sci. Soc. Am. J., 44, 892–898,
795   https://doi.org/10.2136/sssaj1980.03615995004400050002x, 1980.

796   Viterbo, P., Beljaars, A., Mahfouf, J.-F., and Teixeira, J.: The representation of soil moisture
797   freezing and its impact on the stable boundary layer, Q. J. R. Meteorol. Soc., 125, 2401–2426,
798   https://doi.org/10.1002/qj.49712555904, 1999.

799   Walvoord, M. A. and Kurylyk, B. L.: Hydrologic Impacts of Thawing Permafrost—A Review,
800   Vadose Zone J., 15, https://doi.org/10.2136/vzj2016.01.0010, 2016.

801   Wasantha Lal, A. M.: Weighted Implicit Finite-Volume Model for Overland Flow, J. Hydraul.
802   Eng., 124, 941–950, https://doi.org/10.1061/(ASCE)0733-9429(1998)124:9(941), 1998.

803   Weismüller, J., Wollschläger, U., Boike, J., Pan, X., Yu, Q., and Roth, K.: Modeling the thermal
804   dynamics of the active layer at two contrasting permafrost sites on Svalbard and on the Tibetan
805   Plateau, The Cryosphere, 5, 741–757, https://doi.org/10.5194/tc-5-741-2011, 2011.

806   Westermann, S., Langer, M., Boike, J., Heikenfeld, M., Peter, M., Etzelmüller, B., and Krinner,
807   G.: Simulating the thermal regime and thaw processes of ice-rich permafrost ground with the
808   land-surface model CryoGrid 3, Geosci. Model Dev., 9, 523–546, https://doi.org/10.5194/gmd-9-
809   523-2016, 2016.

810   Zhang, T., Barry, R. G., Knowles, K., Heginbottom, J. A., and Brown, J.: Statistics and
811   characteristics of permafrost and ground-ice distribution in the Northern Hemisphere, Polar
812   Geogr., 31, 47–68, https://doi.org/10.1080/10889370802175895, 2008.

813